

Commun. Theor. Phys. **74** (2022) 095404 (8pp) https://doi.org/10.1088/1572-9494/ac80ed

Thawing k-essence dark energy in the PAge space

Zhiqi Huang

School of Physics and Astronomy, Sun Yat-sen University, 2 Daxue Road, Tangjia, Zhuhai 519082, China
CSST Science Center for the Guangdong-Hongkong-Macau Greater Bay Area, Sun Yat-sen University, 2 Daxue Road, Tangjia, Zhuhai 519082, China

E-mail: huangzhq25@mail.sysu.edu.cn

Received 21 April 2022, revised 22 June 2022
Accepted for publication 14 July 2022
Published 29 August 2022

Abstract

A broad class of dark energy models can be written in the form of k-essence, whose Lagrangian density is a two-variable function of a scalar field ϕ and its kinetic energy $X \equiv \frac{1}{2}\partial^\mu\phi\partial_\mu\phi$. In the thawing scenario, the scalar field becomes dynamic only when the Hubble friction drops below its mass scale in the late Universe. Thawing k-essence dark energy models can be randomly sampled by generating the Taylor expansion coefficients of its Lagrangian density from random matrices [Huang Z 2021 *Phys. Rev.* D **104** 103533]. Reference [Huang Z 2021 *Phys. Rev.* D **104** 103533] points out that the non-uniform distribution of the effective equation of state parameters (w_0, w_a) of the thawing k-essence model can be used to improve the statistics of model selection. The present work studies the statistics of thawing k-essence in a more general framework that is Parameterized by the Age of the Universe (PAge) [Huang Z 2020 *Astrophys. J. Lett.* **892** L28]. For fixed matter fraction Ω_m, the random thawing k-essence models cluster in a narrow band in the PAge parameter space, providing a strong theoretical prior. We simulate cosmic shear power spectrum data for the Chinese Space Station Telescope optical survey, and compare the fisher forecast with and without the theoretical prior of thawing k-essence. For an optimal tomography binning scheme, the theoretical prior improves the figure of merit in PAge space by a factor of 3.3.

Keywords: dark energy, cosmological parameters, large-scale structure of universe

(Some figures may appear in colour only in the online journal)

1. Introduction

Since the discovery of the accelerated expansion of the late Universe [3–5], it has been widely accepted that the current Universe is dominated by a dark energy component with negative pressure, whose microscopic nature is often interpreted as a cosmological constant (vacuum energy) that is conventionally denoted as Λ. Over the past two decades, the standard six-parameter Λ cold dark matter (ΛCDM) model has been confronted with a host of observational tests. The high-precision measurements of the temperature and polarization anisotropies of the cosmic microwave background (CMB) provide so far the most stringent constraints on the cosmological parameters [6, 7], which agree well with many other observations such as the baryon acoustic oscillations [8–12], the Type Ia supernovae (SN) [13, 14], the redshift-space distortion [15, 16], and the cosmic chronometers (CC) [17–24].

Despite the observational success, the extraordinary smallness of the vacuum energy (fine-tuning problem) and the coincidence that Λ dominates the Universe only recently (coincidence problem) have, at least philosophically, disturbed cosmologists for decades [25]. Moreover, as the accuracy of observations improves, the great observational success of the ΛCDM model is now challenged by a few anomalies. For instance, the Hubble constant H_0 inferred from CMB + ΛCDM is in $\sim 5\sigma$ tension with the distance-ladder measurements [26, 27]. Less significant challenges include a 3.4σ tension in the matter density fluctuation parameter S_8 between CMB and some cosmic shear data [28–30], a 2.8σ excess of lensing smearing in the CMB power spectra [7], and the lack of

large-angle correlation in CMB temperature [31–34], etc. See [35] for a recent comprehensive review of the observational challenges to the ΛCDM model.

Given that Λ might not be the ultimate truth, we are well motivated to construct alternative dark energy models. A simple and in some sense also minimal construction is to introduce a scalar degree of freedom. Because high-order derivative theories typically suffer from the Ostrogradsky instability [36], it is often assumed that the Lagrangian density only depends on the scalar field value and its kinetic energy $X = \frac{1}{2}\partial_\mu\phi\partial^\mu\phi$. This class of dark energy models, often dubbed as k-essence models, allows a variety of cosmological solutions with rich phenomena [37–73]. In the early time when k-essence dark energy was first proposed, interests were more focused on using the so-called tracking solutions, where the field has attractor-like dynamics in the early Universe, to resolve the coincidence problem [74–77]. It was understood later that the tracking k-essence models are not very successful solutions to the coincidence problem, because they require additional fine-tuning and superluminal fluctuations [78–80]. Moreover, tracking models typically predict moderate deviation from Λ, which is more and more disfavored as the accuracy of observations improves [7, 81]. Alternatively, one can consider the so-called thawing k-essence [1, 82–85], whose mass scale is close to or less than the current expansion rate of the Universe. In the thawing picture, the k-essence field is frozen by the large Hubble friction in the early Universe. Only at low redshift when the expansion rate drops below its mass scale, the field starts to roll. The lightness assumption (mass $\lesssim H_0$) of thawing k-essence naturally leads to non-clustering dark energy whose perturbations are suppressed on sub-horizon scales. There do exist, however, models of dark energy with noticeable sub-horizon perturbations [86–91]. In the present work we do not discuss clustering dark energy models, as they typically need to be treated in a one-by-one manner.

The assumption of a thawing scenario significantly reduces the model complexity. Generating the Taylor expansion coefficients of $\mathcal{L}(\phi, X)$ from random matrices [1], shows that a majority of k-essence dark energy models follows an approximate consistency relation $w_a \approx -1.42\left(\frac{\Omega_m}{0.3}\right)^{0.64}(1 + w_0)$, where Ω_m is the present matter density fraction and w_0, w_a are the Chevallier–Polarski–Linder (CPL) parameters for dark energy equation of state (EOS) [92, 93]. The consistency relation can be understood as follows. Due to the thawing nature, the present rolling speed of the scalar field, which is characterized by $1 + w_0$, is typically correlated to the acceleration of late-time rolling, which is characterized by w_a.

The approximate consistency relation can be combined with observational data to improve the constraining power of cosmological data, which is often measured with the so-called figure of merit in marginalized w_0–w_a space. For a concrete model, however, the dark EOS does not exactly follow the CPL form $w(a) = w_0 + w_a(1 - a)$, where a denotes the scale factor. The parameters w_0, w_a therefore only have an approximate meaning and should be considered as an effective description of dark energy at low redshift. In the present work, we consider another effective description of dark energy with the Parameterization based on cosmic Age (PAge) [2, 94–99]. Compared to the CPL w_0–w_a effective description, PAge does not suffer from a strong parameter degeneracy that is commonly found between w_0 and w_a. Thus, the parameter space of PAge is more compact. The Figure of Merit for the parameterization based on cosmic Age, which we abbreviate as FROMAge to show our French taste, is an equally good, if not better, indicator of the constraining power of cosmological data.

The article is organized as follows. section 2 briefly reviews PAge cosmology. In section 3, we use the numerical tool developed in [1] to generate an ensemble of random thawing k-essence dark energy models, which are then mapped into PAge parameter space. In section 4, we take a future cosmic shear survey as a working example to quantify by how much the thawing k-essence prior may improve the constraining power of cosmological data section 5 concludes. Throughout the paper we work with natural units $c = \hbar = 1$ and a spatially-flat Universe with Friedmann–Lemaître–Robertson–Walker background. The cosmological time and Hubble parameter are denoted as t and H, respectively. The dark EOS is denoted as w, which in general is a function of redshift z. A dot represents derivative with respect to the cosmological time. The current scale factor is normalized to unity. The Hubble constant is denoted as $H_0 = 100h\ \mathrm{km\ s^{-1}\ Mpc^{-1}}$. The square root of the cosmic variance of the mean density in a sphere with radius $8h^{-1}$ Mpc is denoted as σ_8, which then defines the $S_8 \equiv \sigma_8\left(\frac{\Omega_m}{0.3}\right)^{0.5}$ parameter.

2. PAge cosmology

At redshift $z \lesssim 100$, where the radiation component can be ignored, PAge approximates the expansion history of the Universe with the following ansatz [2]

$$\frac{H}{H_0} = 1 + \frac{2}{3}\left(1 - \eta\frac{H_0 t}{p_{\rm age}}\right)\left(\frac{1}{H_0 t} - \frac{1}{p_{\rm age}}\right), \tag{1}$$

where $p_{\rm age} = H_0 t_0$ is the age of the Universe measured in units of H_0^{-1} and $\eta < 1$ is a phenomenological parameter approximately describing the deviation from an Einstein de-Sitter Universe.

Although it may seem like a casual assumption, the PAge ansatz (1) makes use of quite a few physical conditions. First of all, the parameters H_0 and $p_{\rm age}$ are physical quantities that can be directly computed for any given physical model. Secondly, ansatz (1) automatically sets the matter-dominated behavior at a high redshift $\left(\lim_{t\to 0^+} Ht = \frac{2}{3}\right)$. Finally, ansatz (1) guarantees that the expansion rate H monotonically decreases as the Universe expands. Thanks to these physically motivated features, PAge well approximates much dark energy and modified gravity models [2, 94], and performs better than many other phenomenological approaches, such as the oft-used polynomial approximation [100].

At the background level, when H_0^{-1} is treated as a time unit, the expansion history is determined by $p_{\rm page}$ and η, and therefore Ω_m is not a parameter in PAge. While perturbation

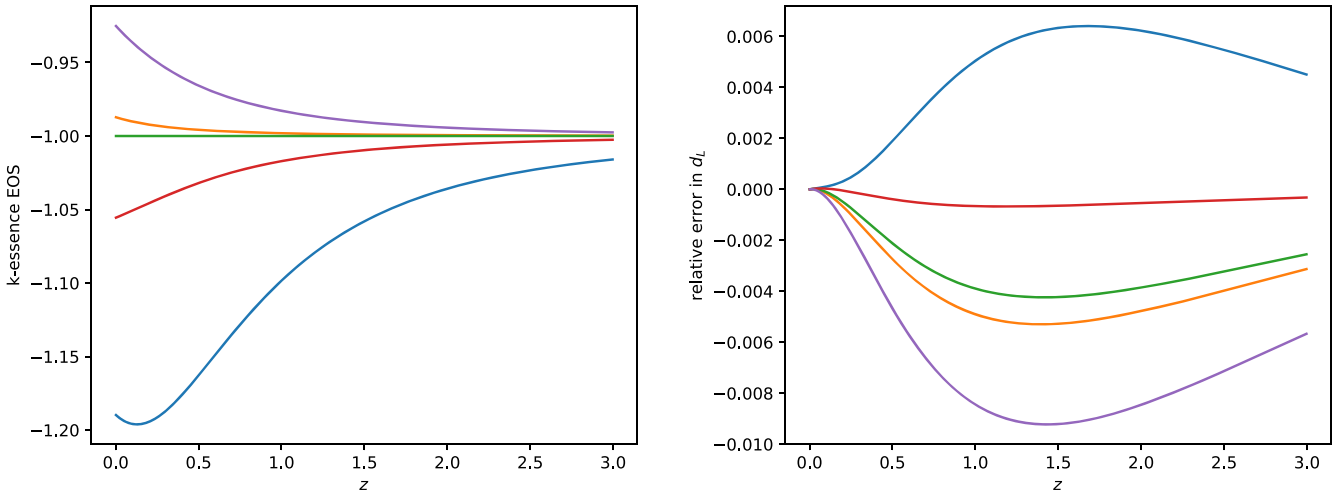

Figure 1. The accuracy of PAge approximation. Left panel: EOS $w(z)$ of a few randomly sampled k-essence dark energy models; right panel: relative error in luminosity distances when the models in the left panel are approximated with PAge. In all cases Ω_m is fixed to 0.3.

Table 1. k-essence generator program settings.

Term in [1]	Program variable	Definition	Value
n	dimX, dimV	Taylor expansion truncation	10
σ	rand_width	Sampling width	3
$k_{\rm pivot}$	khMpc_pivot	Wavenumber to compute perturbations	0.05
Ultraviolet stability	min_cs2	Lower bound for sound speed	0
Acceleration	max_w	Upper bound for dark energy EOS	$-\frac{1}{3}$
Smoothness	max_growth	Upper bound for growth of perturbations	100
Thawing condition	frozen_cut	Upper bound for early-Universe $\lvert 1+w\rvert$	0.01

calculation is needed for the simulation of the cosmic shear data, we add Ω_m to the PAge framework and employ the following linear growth equation

$$\frac{{\rm d}^2D}{{\rm d}t^2}+2H\frac{{\rm d}D}{{\rm d}t}-\frac{3H_0^2}{2a^3}\Omega_m D=0. \tag{2}$$

The assumption that goes into the above equation is that dark energy perturbations at sub-horizon and linear scales can be ignored.

Although more sophisticated approaches exist, for simplicity and to show the robustness of PAge approximation, we follow the simple method in [2] to map dark energy models to PAge space. The η parameter is calculated using the deceleration parameter $q\equiv-\frac{a\ddot{a}}{\dot{a}^2}$ evaluated at redshift zero.

3. Thawing k-essence in PAge space

We use the numerical tool developed in [1], which has been made publicly available at http://zhiqihuang.top/codes/scan_kessence.tar.gz, to generate random k-essence dark energy models. The program settings are shown in table 1. See also [1] for more detailed documentation of the program parameters.

It has been shown in [1], and also tested in the present work, that increasing the truncation order and the sampling width do not change the distribution of sampled trajectories much. This is because models with increasing complexity typically violate the thawing condition ($\lvert 1+w\rvert\ll 1$ in the early Universe), the acceleration assumption $\left(w<-\frac{1}{3}\right)$ or the smoothness assumption (growth of density contrast $\lesssim 10^2$), and thus are rejected by the program.

We generate 41 000 random k-essence dark energy models for a flat prior $\Omega_m\in[0.25, 0.35]$. The models are then mapped into PAge space to generate a joint distribution of ($p_{\rm page}$, η, Ω_m), which we refer to as the thawing k-essence prior. The mapping procedure comes with a tiny accuracy loss in predictions of cosmological observables. In the left panel of figure 1, we show a few k-essence dark energy EOS trajectories with different colors. The relative difference between the luminosity distances predicted from each model and that from its PAge approximation is shown with the same color in the right panel. The errors are typically at a sub-percent level. These tiny errors may be relevant for future cosmological surveys and can be corrected with a more sophisticated approach [97]. We nevertheless work in the original simple PAge framework that is easier to interpret, because the main purpose of the present work is to study the impact of the thawing k-essence prior, rather than the accuracy of PAge approximation.

Due to parameter degeneracy, if the dark energy EOS is a free function of redshift, an exact reconstruction of Ω_m from the expansion history of the Universe is impossible. Since the Lagrangian density $\mathcal{L}(\phi, X)$ is a free function, the EOS of k-essence is almost free, too. However, when the aforementioned physical assumptions are applied, the EOS of thawing

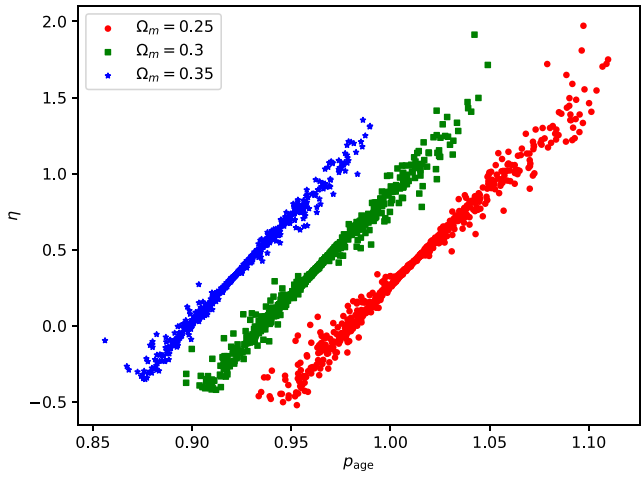

Figure 2. Randomly sampled k-essence dark energy models mapped into the PAge space.

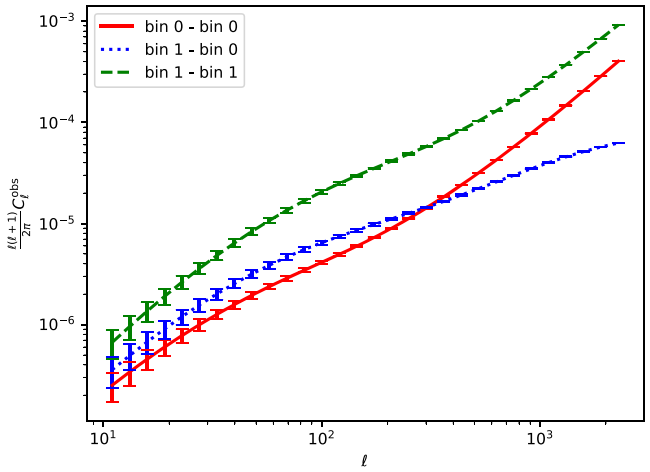

Figure 3. Simulated cosmic shear data with two redshift bins: $z \in [0, 1]$ (bin 0) and $z \in [1, 3]$ (bin 1).

k-essence dark energy is not free in a statistical sense. In figure 2 we compare the mapped ($p_{\rm age}$, η) samples for $\Omega_m = 0.25$, 0.3 and 0.35, respectively. It is evident that one can obtain a statistical constraint on Ω_m from the evolution history that is determined by ($p_{\rm age}$, η). This is a non-trivial result. For a cosmic shear survey, the additional information on Ω_m can break the strong degeneracy between Ω_m and σ_8 and lead to a better reconstruction of low-redshift physics. To make the idea more concrete, in the next section we take a future cosmic shear survey as a working example to quantify the impact of the thawing k-essence prior.

4. Cosmic shear fisher forecast

To make the analysis simple and easy to interpret, we only consider the statistics of the convergence field. The angular power spectrum between the redshift bins i and j is given by the Limber approximation [101–104]

$$C_{\ell;i,j} = \int_0^\infty W_i(z)\, W_j(z) P_m\left(k = \frac{\ell}{\chi(z)}; z\right) \frac{{\rm d}\chi}{{\rm d}z}\, {\rm d}z, \qquad (3)$$

where the comoving angular diameter distance in a spatially flat Universe is given by

$$\chi(z) = \int_0^z \frac{{\rm d}z'}{H(z')}. \qquad (4)$$

The nonlinear matter power spectrum at redshift z, $P_m(k; z)$ where k denotes the wavenumber, is calculated with the Bardeen–Bond–Kaiser–Szalay fitting formula [105] and the halo-fit formula [106, 107]. The weight function in the ith bin $z \in [z_i^{\rm min}, z_i^{\rm max}]$ is given by

$$W_i(z) = \begin{cases} \dfrac{3}{2}\Omega_m H_0^2 (1+z) \dfrac{1}{\bar{n}_i} \displaystyle\int_{\max(z, z_i^{\rm min})}^{z_i^{\rm max}} \left(1 - \frac{\chi(z)}{\chi(z')}\right) \frac{{\rm d}n}{{\rm d}z'} {\rm d}z', & \text{if } z < z_i^{\rm max}, \\ 0, & \text{if } z \geqslant z_i^{\rm max}, \end{cases} \qquad (5)$$

Table 2. Redshift binning schemes.

Number of redshift bins	Bin boundaries
3	0, 0.5, 1, 3
4	0, 0.5, 1, 1.5, 3
5	0, 0.4, 0.8, 1.2, 1.6, 3
8	0, 0.25, 0.5, 0.75, 1, 1.25, 1.5, 1.75, 3

where $\frac{{\rm d}n}{{\rm d}z}$ is the observed galaxy number per unit sky area per unit redshift. The observed galaxy number density in the ith bin is an integral

$$\bar{n}_i = \int_{z_i^{\rm min}}^{z_i^{\rm max}} \frac{{\rm d}n}{{\rm d}z} {\rm d}z. \qquad (6)$$

The total number density of observed galaxies is then the sum $n_{\rm total} = \sum_i n_i$.

The observed convergence power spectrum with shot noise is modeled as

$$C_{\ell;i,j}^{\rm obs} = C_\ell + \frac{\sigma_\epsilon^2}{\bar{n}_i} \delta_{ij}, \qquad (7)$$

where δ_{ij} is the Kronecker delta function and σ_ϵ is the root mean square of the Galaxy intrinsic ellipticity.

For the angular scales we take a conservative multipole range $10 \leqslant \ell \leqslant 2500$. Due to the central limit theorem, the integrated convergence fields over this range are quite close to Gaussian [108–110], and therefore can be written as

$$\begin{aligned} {\rm Cov}[C_{\ell_1;i_1,j_1}^{\rm obs}, C_{\ell_2;i_2,j_2}^{\rm obs}] = & \frac{\delta_{\ell_1\ell_2}}{(2\ell_1+1) f_{\rm sky}} \\ & \times (C_{\ell_1;i_1,i_2}^{\rm obs} C_{\ell_2;j_1,j_2}^{\rm obs} + C_{\ell_1;i_1,j_2}^{\rm obs} C_{\ell_2;i_2,j_1}^{\rm obs}), \end{aligned} \qquad (8)$$

where $f_{\rm sky}$ is the fraction of sky that is observed.

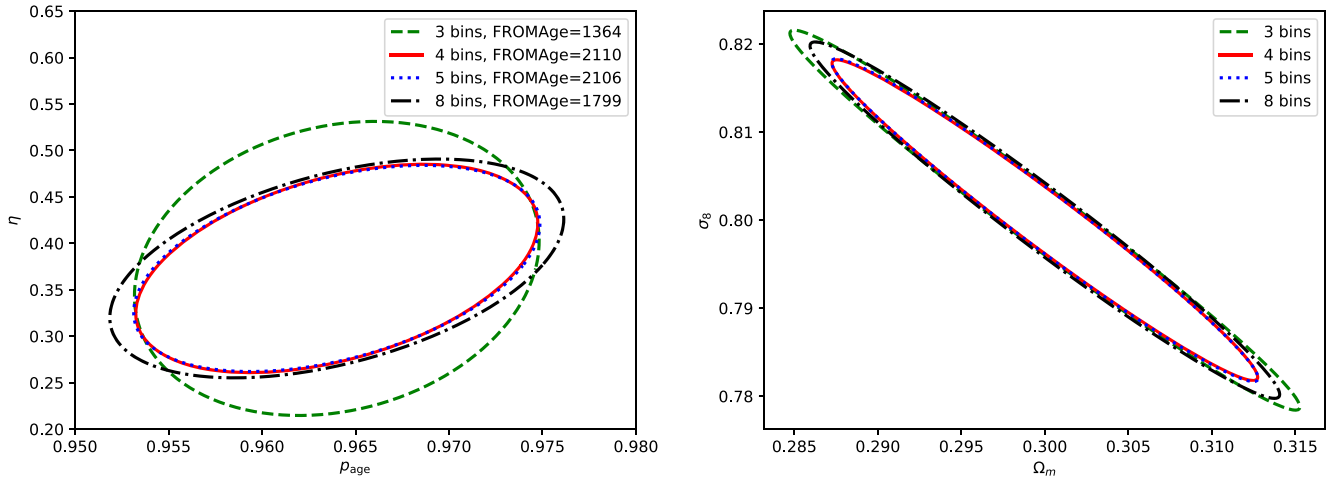

Figure 4. Fisher forecast for different numbers of tomography bins. Photometric redshift error is taken to be $0.03(1+z)$.

If the cosmological redshifts of galaxies were all perfectly known, an optimal analysis would be done within the limit of taking infinitely many redshift bins. In practice, however, the redshift of a photometric survey has a large uncertainty, which in our simulation is assumed to be $\sigma(z) = 0.03(1+z)$. Conventionally when doing a Fisher forecast, the photo-z errors are treated by marginalizing some shift parameters and spreading parameters [104, 111], and the result inevitably depends on many assumptions that are difficult to justify at the stage of forecasting. To make the result robust and easy to interpret, we take a very conservative approach by simply discarding the galaxies samples around the edges of the redshift bins. More concretely, we cut each redshift bin $[z_i^{\rm min}, z_i^{\rm max}]$ to a smaller one $[z_i^{\rm min} + \sigma(z_i^{\rm min}), z_i^{\rm max} - \sigma(z_i^{\rm min})]$. This approach is conservative because we have assumed almost no knowledge about the photo-z error distribution function, which in realistic surveys will be known to some extent.

We have assumed that many other subtle effects such as the intrinsic alignment contamination [112], catastrophic redshift outliers [113], and the super-sample covariance [114] can be well calibrated. The reader is referred to [113, 115–119] for a more detailed discussion about the calibration of these systematics.

In our simulation we assume a galaxy intrinsic ellipticity $\sigma_\epsilon = 0.3$, a galaxy distribution $n(z) \propto z^2 {\rm e}^{-z/0.3}$ that is normalized by $n_{\rm total} = 28$ arcmin^{-2}, and a sky coverage $f_{\rm sky} = 0.424$. The configuration roughly corresponds to the optical survey that will be carried out by the Chinese Space Station Telescope [120]. In figure 3, we show the simulated $C_\ell^{\rm obs}$ and their standard deviations for two redshift bins and thirty ℓ-bins.

We employ the Fisher forecast approach to compute the constraining power on the five dimensional parameter vector: $\theta = (p_{\rm age}, \eta, h, \Omega_m, \sigma_8)$. The Fisher matrix is given by

$$F_{IJ} = \frac{\partial d^{\rm T}}{\partial \theta_I} {\rm Cov}^{-1} \frac{\partial d^{\rm T}}{\partial \theta_J}, \tag{9}$$

where the data vector d is the collection of the observed power spectra $C_{\ell;i,j}^{\rm obs}$ and Cov is the covariance matrix given in equation (8). The covariance of the parameter vector is estimated with the inverse of the Fisher matrix, ${\rm Cov}(\theta_I, \theta_J) \approx (F^{-1})_{IJ}$.

We first study the dependence of the result on the number of redshift bins by comparing four binning schemes listed in table 2.

The marginalized 68.3% confidence-level constraints for $(p_{\rm age}, \eta)$, as well as the FROMAges for the four binning schemes are shown in the left panel of figure 4. As we increase the number of redshift bins, the constraining power (FROMAge) increases at the beginning, and then drops when the photometric redshift error comes into play. A similar tendency is also observed for the other cosmological parameters, such as the (σ_8, Ω_m) combination presented in the right panel of figure 4.

Finally, we apply the thawing k-essence prior in the Fisher analysis. We first bin and interpolate a prior likelihood $P(\Omega_m, p_{\rm age}, \eta)$ from the random samples obtained in the previous section. A full likelihood is obtained by multiplying the data likelihood by the prior likelihood. We run Monte Carlo Markov Chain simulations to obtain the posterior covariance matrix, which is plotted in figure 5 against the original Fisher forecast without thawing k-essence prior. For $(p_{\rm age}, \eta)$ the thawing k-essence prior improves the FROMAge by a factor of 3.3. A similar improvement is found for (σ_8, Ω_m), too.

5. Conclusions

We have shown, with a simple Fisher forecast of future cosmic shear survey, that a reasonable theoretical prior of dark energy can significantly improve the constraining power of the data. This raises the question of whether it is proper to judge the future dark energy surveys with a blind figure of merit without any theoretical prejudice. After all, the history of science has proven that theoretical prejudice is sometimes beneficial.

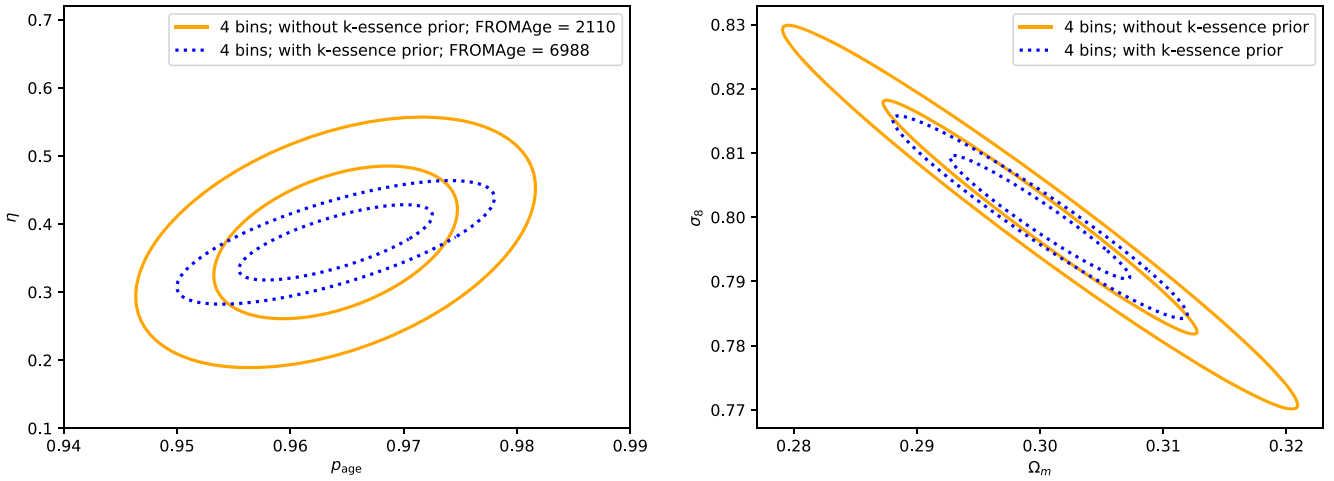

Figure 5. Fisher forecast of the 1σ and 2σ constraints on cosmological parameters, with and without thawing k-essence prior.

Acknowledgments

This work is supported by the National Natural Science Foundation of China (NSFC) under Grant No. 12 073 088, National SKA Program of China No. 2020SKA0110402, National key R&D Program of China (Grant No. 2020YFC2201600), and Guangdong Major Project of Basic and Applied Basic Research (Grant No. 2019B030302001).

ORCID iDs

Zhiqi Huang https://orcid.org/0000-0002-1506-1063

References

[1] Huang Z 2021 Statistics of thawing k-essence dark energy models *Phys. Rev.* D **104** 103533
[2] Huang Z 2020 Supernova magnitude evolution and page approximation *Astrophys. J. Lett.* **892** L28
[3] Riess A G *et al* 1998 Observational evidence from supernovae for an accelerating Universe and a cosmological constant *Astron. J.* **116** 1009–38
[4] Schmidt B P *et al* 1998 The high-z supernova search: measuring cosmic deceleration and global curvature of the Universe using type IA supernovae *Astrophys. J.* **507** 46–63
[5] Perlmutter S *et al* 1998 Measurements of ω and λ from 42 high redshift supernovae *Astrophys. J.* **517** 565–86
[6] Hinshaw G *et al* 2013 Nine-year wilkinson microwave anisotropy probe (WMAP) observations: cosmological parameter results *Astrophys. J. Suppl.* **208** 19
[7] Aghanim N *et al* 2020 Planck 2018 results. VI. Cosmological parameters *Astron. Astrophys.* **641** A6
[8] Beutler F, Blake C, Colless M, Jones D H, Staveley-Smith L, Campbell L, Parker Q, Saunders W and Watson F 2011 The 6dF galaxy survey: baryon acoustic oscillations and the local hubble constant *Mon. Not. Roy. Astron. Soc.* **416** 3017–32
[9] Alam S *et al* 2017 The clustering of galaxies in the completed SDSS-III baryon oscillation spectroscopic survey: cosmological analysis of the DR12 galaxy sample *Mon. Not. Roy. Astron. Soc.* **470** 2617–52
[10] du Mas des Bourboux H *et al* 2017 Baryon acoustic oscillations from the complete SDSS-III Lyα-quasar cross-correlation function at $z = 2.4$ *Astron. Astrophys.* **608** A130
[11] Ata M *et al* 2018 The clustering of the SDSS-IV extended baryon oscillation spectroscopic survey dr14 quasar sample: first measurement of baryon acoustic oscillations between redshift 0.8 and 2.2 *Mon. Not. Roy. Astron. Soc.* **473** 4773–94
[12] Alam S *et al* 2021 Completed SDSS-IV extended baryon oscillation spectroscopic survey: cosmological implications from two decades of spectroscopic surveys at the apache point observatory *Phys. Rev.* D **103** 083533
[13] Betoule M *et al* 2014 Improved cosmological constraints from a joint analysis of the SDSS-II and SNLS supernova samples *Astron. Astrophys.* **568** A22
[14] Scolnic D M *et al* 2018 The complete light-curve sample of spectroscopically confirmed SNe Ia from Pan-STARRS1 and cosmological constraints from the combined pantheon sample *Astrophys. J.* **859** 101
[15] Nadathur S *et al* 2020 The completed SDSS-IV extended baryon oscillation spectroscopic survey: geometry and growth from the anisotropic void-galaxy correlation function in the luminous red galaxy sample *Mon. Not. Roy. Astron. Soc.* **499** 4140–57
[16] Pezzotta A *et al* 2017 The VIMOS public extragalactic redshift survey (VIPERS): the growth of structure at $0.5 < z < 1.2$ from redshift-space distortions in the clustering of the PDR-2 final sample *Astron. Astrophys.* **604** A33
[17] Jimenez R and Loeb A 2002 Constraining cosmological parameters based on relative galaxy ages *Astrophys. J.* **573** 37–42
[18] Simon J, Verde L and Jimenez R 2005 Constraints on the redshift dependence of the dark energy potential *Phys. Rev.* D **71** 123001
[19] Stern D, Jimenez R, Verde L, Kamionkowski M and Stanford S A 2010 Cosmic chronometers: constraining the equation of state of dark energy. I: H(z) measurements *J. Cosmol. Astropart. Phys.* JCAP02(2010)008
[20] Zhang C, Zhang H, Yuan S, Zhang T-J and Sun Y-C 2014 Four new observational $H(z)$ data from luminous red galaxies in the Sloan Digital Sky Survey data release seven *Res. Astron. Astrophys.* **14** 1221–33
[21] Moresco M *et al* 2012 Improved constraints on the expansion rate of the Universe up to z̃1.1 from the spectroscopic evolution of cosmic chronometers *J. Cosmol. Astropart. Phys.* JCAP08(2012)006
[22] Moresco M 2015 Raising the bar: new constraints on the Hubble parameter with cosmic chronometers at z ∼2 *Mon. Not. Roy. Astron. Soc.* **450** L16–20

[23] Moresco M, Pozzetti L, Cimatti A, Jimenez R, Maraston C, Verde L, Thomas D, Citro A, Tojeiro R and Wilkinson D 2016 A 6% measurement of the Hubble parameter at $z \sim 0.45$: direct evidence of the epoch of cosmic re-acceleration *J. Cosmol. Astropart. Phys.* JCAP05(2016)014

[24] Ratsimbazafy A L *et al* 2017 Age-dating luminous red galaxies observed with the southern african large telescope *Mon. Not. Roy. Astron. Soc.* **467** 3239–54

[25] Weinberg S 1989 The cosmological constant problem *Rev. Mod. Phys.* **61** 1–23

[26] Riess A G, Casertano S, Yuan W, Bowers J B, Macri L, Zinn J C and Scolnic D 2021 Cosmic distances calibrated to 1% precision with gaia edr3 parallaxes and hubble space telescope photometry of 75 milky way cepheids confirm tension with ΛCDM *Astrophys. J. Lett.* **908** L6

[27] Riess A G *et al* 2021 A comprehensive measurement of the local value of the Hubble Constant with 1 km/s/Mpc uncertainty from the hubble space telescope and the SH0ES TeamarXiv:2112.04510

[28] Asgari M *et al* 2021 KiDS-1000 cosmology: cosmic shear constraints and comparison between two point statistics *Astron. Astrophys.* **645** A104

[29] van den Busch J L *et al* 2022 KiDS-1000: cosmic shear with enhanced redshift calibration arXiv:2204.02396

[30] Amon A *et al* 2022 Consistent lensing and clustering in a low-S_8 Universe with BOSS, DES Year 3, HSC Year 1 and KiDS-1000 arXiv:2202.07440

[31] Hinshaw G, Branday A J, Bennett C L, Gorski K M, Kogut A, Lineweaver C H, Smoot G F and Wright E L 1996 Two-point correlations in the cobe dmr four-year anisotropy maps *Astrophys. J. Lett.* **464** L25

[32] Bennett C L *et al* 2003 The microwave anisotropy probe mission *Astrophys. J.* **583** 1–23

[33] Efstathiou G, Ma Y-Z and Hanson D 2010 Large-angle correlations in the cosmic microwave background *MNRAS* **407** 2530–42

[34] Ade P A R *et al* 2016 Planck 2015 results. XVI. Isotropy and statistics of the CMB *A&A* **594** A16

[35] Perivolaropoulos L and Skara F 2022 Challenges for ΛCDM: an update *New Astron. Rev.* **95** 101659

[36] Ostrogradsky M 1850 Mémoires sur les équations différentielles, relatives au problème des isopérimètres *Mem. Acad. St. Petersbourg, series* **6** 385

[37] Chiba T, Okabe T and Yamaguchi M 2000 Kinetically driven quintessence *Phys. Rev.* D **62** 023511

[38] Malquarti M, Copeland E J, Liddle A R and Trodden M 2003 A new view of k-essence *Phys. Rev.* D **67** 123503

[39] Chimento L P and Feinstein A 2004 Power-low expansion in k-ESSENCE cosmology *Mod. Phys. Lett.* A **19** 761–8

[40] Aguirregabiria J M, Chimento L P and Lazkoz R 2004 Phantom k-essence cosmologies *Phys. Rev.* D **70** 023509

[41] Chimento L P and Lazkoz R 2005 Atypical k-essence cosmologies *Phys. Rev.* D **71** 023505

[42] Kim H 2005 Brans Dicke scalar field as a unique k-essence *Phys. Lett.* B **606** 223–33

[43] Lazkoz R 2005 Rigidity of cosmic acceleration in a class of k-ESSENCE cosmologies *Int. J. Mod. Phys.* D **14** 635–41

[44] Aguirregabiria J M, Chimento L P and Lazkoz R 2005 Quintessence as k-essence [rapid communication] *Phys. Lett.* B **631** 93–9

[45] Chimento L P and Forte M 2006 Anisotropic k-essence cosmologies *Phys. Rev.* D **73** 063502

[46] Rendall A D 2006 Dynamics of k-essence *Class. Quant. Gravity* **23** 1557–69

[47] Chimento L P and Lazkoz R 2006 Crossing the phantom barrier with purely kinetic multiple k-essence *Phys. Lett.* B **639** 591–5

[48] de Putter R and Linder E V 2007 Kinetic k-essence and quintessence *Astropart. Phys.* **28** 263–72

[49] Cruz N, González-Díaz P F, Rozas-Fernández A and Sánchez G 2009 Holographic kinetic k-essence model *Phys. Lett.* B **679** 293–7

[50] Gao X-T and Yang R-J 2010 Geometrical diagnostic for purely kinetic k-essence dark energy *Phys. Lett.* B **687** 99–102

[51] Chimento L P, Forte M and Richarte M G 2010 Crossing the phantom divide with k-ESSENCE in braneworlds *Mod. Phys. Lett.* A **25** 2469–81

[52] Bouhmadi-López M and Chimento L P 2010 k-essence in the DGP brane-world cosmology *Phys. Rev.* D **82** 103506

[53] Chimento L P and Richarte M G 2011 k-ESSENCE and tachyons in braneworld cosmology *Int. J. Mod. Phys.* D **20** 1705–12

[54] Deffayet C, Gao X, Steer D A and Zahariade G 2011 From k-essence to generalized Galileons *Phys. Rev.* D **84** 064039

[55] Tsyba P Y, Kulnazarov I I, Yerzhanov K K and Myrzakulov R 2011 Pure kinetic K-essence as the cosmic speed-up *Int. J. Theor. Phys.* **50** 1876–86

[56] Myrzakulov R 2012 Cosmology of F(T) gravity and k-essence *Entropy* **14** 1627–51

[57] Myrzakulov R 2012 F(T) gravity and k-essence *Gen. Relativ. Gravitation* **44** 3059–80

[58] De-Santiago J and Cervantes-Cota J L 2012 On the dynamics of unified k-essence cosmologies *IX Workshop of the Gravitation and Mathematical Physics Division of the Mexican Physical Society, vol 1473 of American Institute of Physics Conf. Series* pp 59–67

[59] Sharif M and Rani S 2011 The k-essence models and cosmic acceleration in generalized teleparallel gravity *Phys. Scr.* **84** 055005

[60] Rozas-Fernández A 2012 Kinetic k-essence ghost dark energy model *Phys. Lett.* B **709** 313–21

[61] Cárdenas V H, Cruz N and Villanueva J R 2015 Testing a dissipative kinetic k-essence model *Eur. Phys. J.* C **75** 148

[62] Graham A A H 2015 Varying-α and k-essence *Class. Quant. Gravity* **32** 015019

[63] Bouhmadi-López M, Kumar K S, Marto J, Morais J and Zhuk A 2016 K-essence model from the mechanical approach point of view: coupled scalar field and the late cosmic acceleration *J. Cosmol. Astropart. Phys.* JCAP16 (2016)050

[64] Myrzakul S, Myrzakulov R and Sebastiani L 2016 k-essence in Horndeski models *Astrophys. Space Sci.* **361** 254

[65] Tannukij L and Wongjun P 2016 Mass-varying massive gravity with k-essence *Eur. Phys. J.* C **76** 17

[66] Guendelman E, Nissimov E and Pacheva S 2016 Unified dark energy and dust dark matter dual to quadratic purely kinetic K-essence *Eur. Phys. J.* C **76** 90

[67] Cordero R, Miranda O G and Serrano-Crivelli M 2019 K-essence and kinetic gravity braiding models in two-field measure theory *J. Cosmol. Astropart. Phys.* JCAP19 (2019)027

[68] Mukherjee S and Gangopadhyay D 2021 An accelerated Universe with negative equation of state parameter in inhomogeneous cosmology with k-essence scalar field *Phys. Dark Univ.* **32** 100800

[69] Shi J and Wu J-P 2021 Dynamics of k-essence in loop quantum cosmology *Chin. Phys.* C **45** 045104

[70] Barvinsky A O, Kolganov N and Vikman A 2021 Generalized unimodular gravity as a new form of k -essence *Phys. Rev.* D **103** 064035

[71] Tian S X and Zhu Z-H 2021 Early dark energy in k -essence *Phys. Rev.* D **103** 043518

[72] Orjuela-Quintana J B and Valenzuela-Toledo C A 2021 Anisotropic k-essence *Phys. Dark Univ.* **33** 100857

[73] Lara G, Bezares M and Barausse E 2022 UV completions, fixing the equations, and nonlinearities in kessence *Phys. Rev.* D **105** 064058

[74] Armendariz-Picon C, Mukhanov V and Steinhardt P J 2000 Dynamical solution to the problem of a small cosmological constant and late-time cosmic acceleration *Phys. Rev. Lett.* **85** 4438–41
[75] Chiba T 2002 Tracking k-essence *Phys. Rev.* D **66** 063514
[76] Armendariz-Picon C, Mukhanov V and Steinhardt P J 2001 Essentials of k-essence *Phys. Rev.* D **63** 103510
[77] Das R, Kephart T W and Scherrer R J 2006 Tracking quintessence and k-essence in a general cosmological background *Phys. Rev.* D **74** 103515
[78] Malquarti M, Copeland E J and Liddle A R 2003 k-essence and the coincidence problem *Phys. Rev.* D **68** 023512
[79] Bonvin C, Caprini C and Durrer R 2006 No-Go theorem for k-essence dark energy *Phys. Rev. Lett.* **97** 081303
[80] Kang J U, Vanchurin V and Winitzki S 2007 Attractor scenarios and superluminal signals in k-essence cosmology *Phys. Rev.* D **76** 083511
[81] Ade P A R *et al* 2016 Planck 2015 results. XIV. Dark energy and modified gravity *A&A* **594** A14
[82] Scherrer R J and Sen A A 2008 Thawing quintessence with a nearly flat potential *Phys. Rev.* D **77** 083515
[83] Chiba T 2009 Slow-roll thawing quintessence *Phys. Rev.* D **79** 083517
[84] Chiba T, Dutta S and Scherrer R J 2009 Slow-roll k-essence *Phys. Rev.* D **80** 043517
[85] Kehayias J and Scherrer R J 2019 New generic evolution for k-essence dark energy with w ≈-1 *Phys. Rev.* D **100** 023525
[86] Feng C-J and Li X-Z 2009 Scalar perturbation and stability of Ricci dark energy *Phys. Lett.* B **680** 184–7
[87] Bueno Sanchez J C and Perivolaropoulos L 2010 Evolution of dark energy perturbations in scalar-tensor cosmologies *Phys. Rev.* D **81** 103505
[88] Gubitosi G, Piazza F and Vernizzi F 2013 The effective field theory of dark energy *J. Cosmol. Astropart. Phys.* JCAP13 (2013)032
[89] Huang Z 2016 Observational effects of a running Planck mass *Phys. Rev.* D **93** 043538
[90] Bellini E *et al* 2018 Comparison of Einstein–Boltzmann solvers for testing general relativity *Phys. Rev.* D **97** 023520
[91] Creminelli P, Tambalo G, Vernizzi F and Yingcharoenrat V 2020 Dark-energy instabilities induced by gravitational waves *J. Cosmol. Astropart. Phys.* JCAP20(2020)002
[92] Chevallier M and Polarski D 2001 Accelerating Universes with scaling dark matter *Int. J. Mod. Phys.* D **10** 213–24
[93] Linder E V 2003 Exploring the expansion history of the Universe *Phys. Rev. Lett.* **90** 091301
[94] Luo X, Huang Z, Qian Q and Huang L 2020 Reaffirming the cosmic acceleration without supernovae and the cosmic microwave background *Astrophys. J.* **905** 53
[95] Huang L, Huang Z, Luo X and Fang Y 2021 Reconciling low and high redshift GRB luminosity correlations *Phys. Rev.* D **103** 123521
[96] Huang L, Huang Z, Zhou H and Li Z 2022 The S_8 tension in light of updated redshift-space distortion data and page approximation *SCPMA* **65** 239512
[97] Huang L, Huang Z-Q, Li Z-Y and Zhou H 2021 A more accurate Parameterization based on cosmic Age (MAPAge) *Res. Astron. Astrophys.* **21** 277
[98] Cai R-G, Guo Z-K, Wang S-J, Yu W-W and Zhou Y 2022 No-go guide for the Hubble tension: Late-time solutions *Phys. Rev.* D **105** L021301
[99] Cai R-G, Guo Z-K, Wang S-J, Yu W-W and Zhou Y 2022 No-go guide for the Hubble tension : matter perturbations arXiv:2202.12214
[100] Visser M 2004 Jerk and the cosmological equation of state *Class. Quant. Gravity* **21** 2603–16
[101] Limber D N 1954 The analysis of counts of the extragalactic nebulae in terms of a fluctuating density field. II *Astrophys. J.* **119** 655
[102] Kaiser N 1992 Weak gravitational lensing of distant galaxies *Astrophys. J.* **388** 272
[103] Kaiser N 1998 Weak lensing and cosmology *Astrophys. J.* **498** 26–42
[104] Hu W 1999 Power spectrum tomography with weak lensing *Astrophys. J. Lett.* **522** L21–4
[105] Bardeen J M, Bond J R, Kaiser N and Szalay A S 1986 The statistics of peaks of gaussian random fields *Astrophys. J.* **304** 15
[106] Smith R E, Peacock J A, Jenkins A, White S D M, Frenk C S, Pearce F R, Thomas P A, Efstathiou G and Couchman H M P 2003 Stable clustering, the halo model and nonlinear cosmological power spectra *MNRAS* **341** 1311–32
[107] Takahashi R, Sato M, Nishimichi T, Taruya A and Oguri M 2012 Revising the halofit model for the nonlinear matter power spectrum *Astrophys. J.* **761** 152
[108] Scoccimarro R and Frieman J A 1999 Hyperextended cosmological perturbation theory: predicting nonlinear clustering amplitudes *Astrophys. J.* **520** 35–44
[109] White M and Hu W 2000 A new algorithm for computing statistics of weak lensing by large-scale structure *Astrophys. J.* **537** 1–11
[110] Cooray A and Hu W 2001 Power spectrum covariance of weak gravitational lensing *Astrophys. J.* **554** 56–66
[111] Ma Z, Hu W and Huterer D 2006 Effects of photometric redshift uncertainties on weak-lensing tomography *Astrophys. J.* **636** 21–9
[112] Takada M and White M 2004 Tomography of lensing cross-power spectra *Astrophys. J. Lett.* **601** L1–4
[113] Huterer D, Takada M, Bernstein G and Jain B 2006 Systematic errors in future weak-lensing surveys: requirements and prospects for self-calibration *MNRAS* **366** 101–14
[114] Takada M and Hu W 2013 Power spectrum super-sample covariance *Phys. Rev.* D **87** 123504
[115] Li Y, Hu W and Takada M 2014 Super-sample covariance in simulations *Phys. Rev.* D **89** 083519
[116] Takada M and Spergel D N 2014 Joint analysis of cluster number counts and weak lensing power spectrum to correct for the super-sample covariance *MNRAS* **441** 2456–75
[117] Takahashi R, Soma S, Takada M and Kayo I 2014 An optimal survey geometry of weak lensing survey: minimizing supersample covariance *MNRAS* **444** 3473–87
[118] Li Y, Hu W and Takada M 2014 Super-sample signal *Phys. Rev.* D **90** 103530
[119] Kilbinger M 2015 Cosmology with cosmic shear observations: a review *Rep. Prog. Phys.* **78** 086901
[120] Gong Y *et al* 2019 Cosmology from the chinese space station optical survey (CSS-OS) *Astrophys. J.* **883** 203